26th Optoelectronics and Communications Conference (OECC)
2021 © OSA 2021

Performance Comparison of Different 8-QAM Constellations Used in SEFDM systems

Peiji Song[1] *, Zhouyi Hu[2], Chun-Kit Chan[1]
[1]*Department of Information Engineering, The Chinese University of Hong Kong, Hong Kong*
[2] *Aston Institute of Photonic Technologies, Aston University, Birmingham, B4 7ET, United Kingdom*
* sp020@ie.cuhk.edu.hk

Abstract: We investigate and compare the performances of three different 8-QAM formats used in SEFDM systems, with respect to the limiting factors of system noises and inter-carrier intereference.

1. Introduction

With the rapid deployment of many emerging smart applications, the demands of bandwidth and transmission speeds in data center interconnects (DCIs) are growing drastically [1]. Among the techniques to support the transmission links in DCIs, intensity modulation with direct detection (IM-DD) is more desirable than coherent detection, due to its cost-effectiveness and simple implementation. In addition to the conventional pulse amplitude modulation (PAM) [2], carrier-less amplitude and phase modulation (CAP) [3], and half-cycle quadrature amplitude modulation (QAM) [4], discrete multi-tone modulation (DMT) [5] is emerged as a flexible modulation technique, which assigns different modulation formats and transmitted powers to different subcarriers, via adaptive bit and power loading algorithms [6]. To further improve the bandwidth utilization, spectrally efficient frequency division multiplexing (SEFDM) has recently been proposed [7]. It achieves a higher spectral efficiency (SE) than DMT by further reducing the subcarrier spacing in the frequency domain beyond the Nyquist limit, at the expense of the violation of the orthogonality among the subcarriers. Due to the loss of orthogonality, inter-carrier interference (ICI) is the major impairment to limit the performance. Although some effective schemes including the cascaded binary-phase-shift-keying iterative decoding (CBID) and the fixed sphere decoder (FSD), have been reported to alleviate the ICI, they are limited to the modulation formats of 4-QAM and 16-QAM transmission [7]. These are attributed to the constraints that CBID is limited to square QAM formats, and fixed sphere decoding (FSD) has very high complexity. However, applying 16-QAM in SEFDM will impose a very high complexity at the receiver, while only utilizing 4-QAM cannot meet the requirement of DCIs with transmission rates larger than 200 Gb/s. To simultaneously achieve a higher transmission rate and maintain relatively low complexity at the receiver, 8-QAM is an appropriate choice that can be employed with 4-QAM and 16-QAM for adaptive SEFDM transmission. When distinct symbol distances and amplitudes are considered [8], 8-QAM allows many possible signal constellations with different performances. Hence, the selection of a suitable 8-QAM format becomes crucial for the implementation of an adaptive SEFDM system.

In this paper, we numerically investigate three different 8-QAM formats for SEFDM systems and compare their performances under different conditions. To directly generate a real-valued signal and give a fair comparison, we employ modified fractional discrete Fourier transform (mFrDFT) proposed in [9] and design three decoding methods for these three 8-QAM formats accordingly with iterative decoding (ID). Simulation results show that under low signal-to-noise ratio (SNR) region and small effective subcarriers number conditions, circular 8-QAM performs better than rectangular 8-QAM, while in high SNR region and the case of a large number of effective subcarriers, rectangular 8-QAM outperforms circular 8-QAM. Meanwhile, star 8-QAM always achieves the best performance. The results show that there is a trade-off between Euclidean distance and the system performance. When additive white Gaussian noise (AWGN) is the limiting factor, higher Euclidean distance is helpful to improve the performance. However, when ICI is the limiting factor, higher Euclidean distance will lead to higher ICI, which will further degrade the performance significantly.

2. Principles of the digital signal processing

Fig. 1 depicts the three 8-QAM formats and their decoding strategies. It shows that circular 8-QAM has the largest Euclidean distance and the rectangular one has the smallest Euclidean distance under the same transmitted power, thus circular 8-QAM format is more robust to AWGN. Given the constraints of CBID and FSD, iterative detection (ID) [10] is adopted as the receiver soft decoder in this work. The ID algorithm is based on the correlation matrix C for $C = F^H F$, where the superscript H denotes the Hermitian transpose operation, and, F is an $(2N+2)\times(2N+2)$ ImFrDFT matrix, given by Eq.(1).

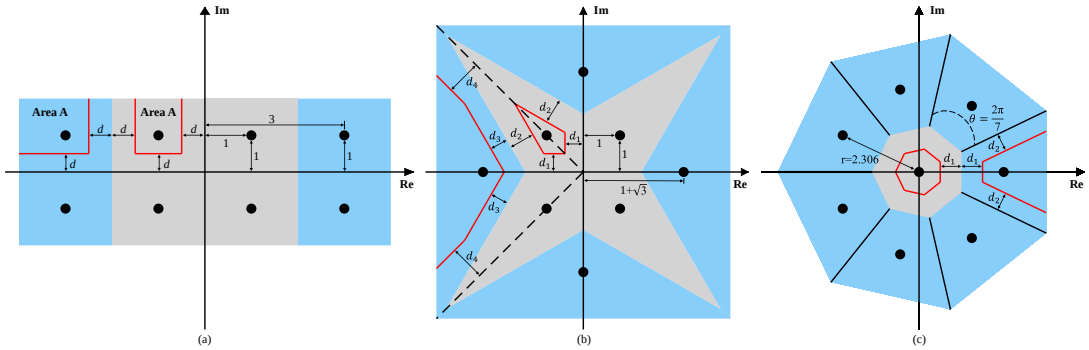

Fig. 1. Mapping strategies for (a) rectangular 8-QAM constellation; (b) star 8-QAM constellation; (c) circular 8-QAM constellation.

$$F=\frac{1}{\sqrt{(2N+2)}}\begin{pmatrix} e^{\beta k_1 n_1} & \cdots & e^{\beta k_1 (N/\alpha-N+n_2)} \\ \vdots & \ddots & \vdots \\ e^{\beta n_1 (N/\alpha-N+k_2)} & \cdots & e^{\beta (N-k_2)(N-n_2)} \end{pmatrix} \tag{1}$$

where $\beta=j2\pi\alpha/(2N+2)$ and α is the bandwidth compression ratio (BCR). $k_1=0,1,\ldots,(N+1)$ and $k_2=(N+2),(N+3),\ldots,(2N+2)$ denote the row indices. $n_1=0,1,\ldots,(N+1)$ and $n_2=(N+2),(N+3),\ldots,(2N+2)$ and denote the column indices. To ensure the symmetry of the frequency distribution of the subcarriers, the elements of the $(N+2)^{th}$ row and that of the $(N+2)^{th}$ column are set to the zero-frequency region. The element $C_{m,n}$ in the correlation matrix C denotes the crosstalk from the n^{th} subcarrier to the m^{th} subcarrier. In the i^{th} iteration of ID, the recovered symbol vector S_i is first updated by Eq.(2).

$$S_i = R-(C-I)S_{i-1} \tag{2}$$

where R is the received symbols after mFrDFT, I is an identity matrix, and S_{i-1} is the recovered symbols after $(i-1)^{th}$ iterations. As shown in Fig. 1, after one ID iteration, only the recovered symbols located inside area A are mapped to the corresponding constellation points, while other symbols stay unchanged for the next iteration. For a fair performance comparison, we design three different mapping strategies for these three 8-QAM formats based on ID.

Fig. 2 depicts the block diagram of the digital processing (DSP) stack in the numerical simulation. In the DSP stack at the transmitter (TX) side, as shown in Fig. 2(a), the random bit stream is first mapped into the 8-QAM symbols. Then, N effective subcarriers with 8-QAM symbols are used to perform Hermitian symmetry for the real-valued SEFDM signal generation by a $(2N+2)$-point ImFrDFT, where only the subcarriers with zero frequency are unfilled [10]. Before the parallel-to-serial conversion, the cyclic prefix (CP) is added, where its length is set to be 1/16 of one SEFDM symbol. Fig. 2(b) shows the DSP stack at the receiver (RX) side, the obtained SEFDM signal is processed by serial-to-parallel conversion, CP removal, channel estimation and the corresponding frequency-domain equalization (FDE), demodulation based on mFrDFT, ICI elimination based on ID algorithms, and finally the 8-QAM symbols demapping and BER calculation.

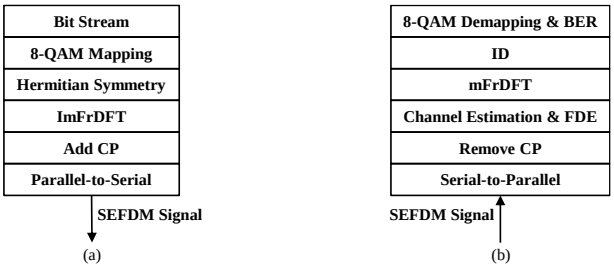

Fig. 2. (a) Transmitter-side DSP stack for the SEFDM 8-QAM signal, (b) receiver-side DSP stack for the SEFDM 8-QAM signal.

3. Results and Discussions

Fig. 3 depicts the simulated BER versus SNR for these three 8-QAM formats with different values of N, where we only consider the back-to-back (BtB) transmission scenario. For a fair comparison, we set the iteration number for all three specially designed ID algorithms to 20. We can notice that for the conventional OFDM case, i.e., $\alpha=1$, the circular 8-QAM format, which has the largest Euclidean distance under the same transmitted power than the other two, performs the best. For the SEFDM signals with $\alpha=0.9$ and $\alpha=0.88$, the rectangular 8-QAM gradually

outperforms the circular 8-QAM when *N* increases, while the star 8-QAM always performs the best. This can be attributed to the trade-off between the Euclidean distance and the performance. Unlike conventional OFDM where there is no ICI, ICI is a critical factor affecting the performance of SEFDM signals and it increases with *N*. The circular 8-QAM has higher ICI than the rectangular and the star 8-QAM under the same transmitted power, due to its larger Euclidean distance. For small values of *N*, the AWGN becomes the limiting factor in the performance. Hence, the circular 8-QAM with a larger Euclidean distance performs better than the rectangular 8-QAM. At low SNR, the circular 8-QAM outperforms the rectangular 8-QAM, while the latter outperforms the former, as the SNR increases.

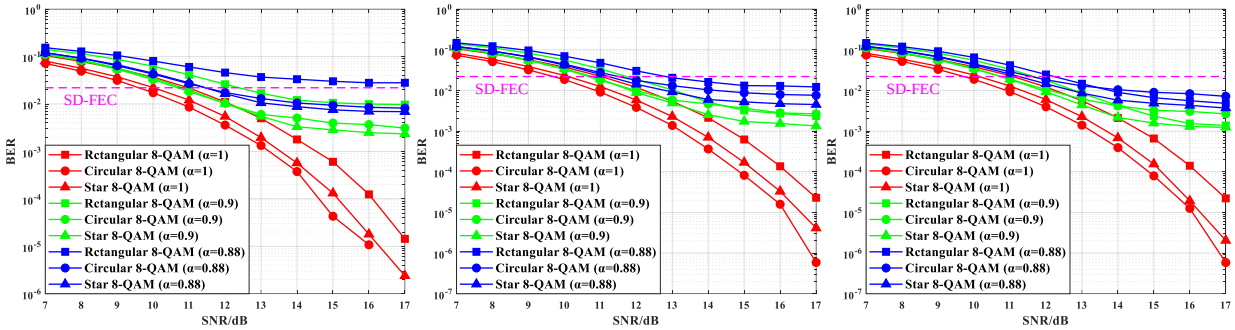

(a) (b) (c)

Fig.3. Simulated BER versus SNR for different BCRs and 8-QAM formats with (a) N=31, (b) N=63 and (c) N=127.

It can also be observed from Fig. 3 that the final performance of SEFDN signals improves when *N* increases. This can be attributed to the crosstalk, as shown in Fig. 4. For a fixed *N*, the ICI becomes more severe as the BCR α decreases. Besides, the crosstalk decreases, with the increase in *N*, thus improves the performance.

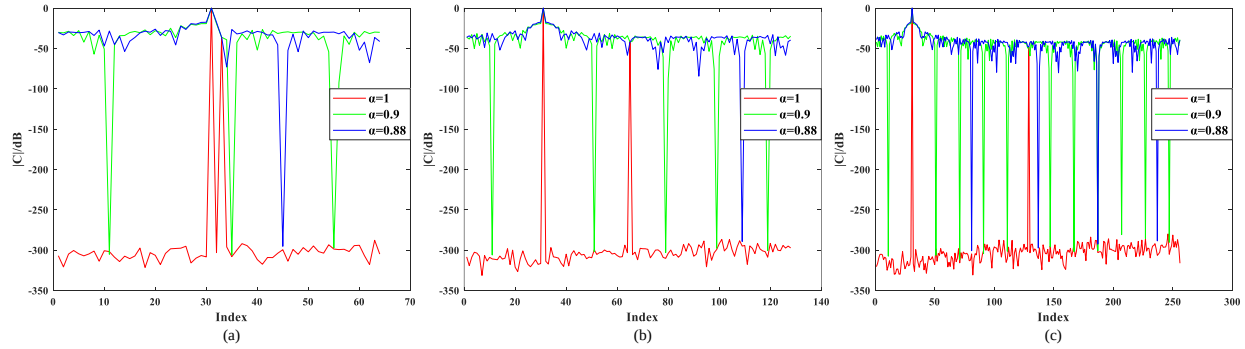

(a) (b) (c)

Fig. 4. (a) Crosstalk matrix $|C_{l,31}|$ versus *l* for *N*=31, (b) Crosstalk matrix $|C_{l,63}|$ versus *l* for *N*=63, (b) Crosstalk matrix $|C_{l,127}|$ versus *l* for *N*=127.

4. Summary

We have compared the performances of three different 8-QAM constellations used in SEFDM systems, with respect to the impact of the SNR and the number of effective subcarriers (*N*), via numerical simulations. The results have shown that there is a trade-off between the Euclidean distance and the final performance. Under low-SNR and small value of *N* conditions, AWGN is the limiting factor and the circular 8-QAM performs better than the rectangular 8-QAM. However, at high SNR and large values of *N*, ICI is the limiting factor and the rectangular 8-QAM outperforms the circular 8-QAM. Meanwhile, under both scenarios, the final performance of the star 8-QAM always performs the best.

5. References

[1] K. Zhong, et al., J. Lightwave Technol. 36(2), 377-400 (2017).
[2] F. Chang, et al., in Proc. ECOC (2017), paper W.1.A.5.
[3] M. I. Olmedo, et al., J. Lightwave Technol. 32(4), 798-804 (2014).
[4] J. Zhou, et al., Opt. Lett., 41(12), 2767-2770 (2016).
[5] Y. Kai, et al., in Proc. ECOC (2013), paper Th.1.F.3.
[6] P. Chow, et al., IEEE Trans. Commun. 43(234), 773–775 (1995).
[7] Z. Hu, et al., J. Lightwave Technol. 38(3), 632-641 (2020).
[8] L. Nadal, et al., IEEE Photon. Lett., 28(4), 445-448 (2016).
[9] Z. Hu, et al., in Proc. ECOC (2018), paper Th2. 18.
[10] Y. Zhu, et al., in Proc. OFC (2019), paper W2A.47.